catalysts

MDPI

Article

Size-Controlled Synthesis of Pt Particles on TiO_2 Surface: Physicochemical Characteristic and Photocatalytic Activity

Anna Zielińska-Jurek [1,*], Zhishun Wei [2,3], Marcin Janczarek [2,4], Izabela Wysocka [1] and Ewa Kowalska [2]

[1] Department of Process Engineering and Chemical Technology, Gdansk University of Technology, Narutowicza 11/12, 80-233 Gdansk, Poland; annjurek@pg.edu.pl (A.Z-J.); izabela.wysocka@pg.edu.pl (I.W.)
[2] Institute for Catalysis (ICAT), Hokkaido University, N21, W10, Sapporo 001-0021, Japan; wei@cat.hokudai.ac.jp (Z.W.); marcin.janczarek@put.poznan.pl (M.J.); kowalska@cat.hokudai.ac.jp (E.W.)
[3] Hubei Provincial Key Laboratory of Green Materials for Light Industry, Hubei University of Technology, Wuhan 430068, China
[4] Institute of Chemical Technology and Engineering, Faculty of Chemical Technology, Poznan University of Technology, 60-965 Poznan, Poland; marcin.janczarek@put.poznan.pl
* Correspondence: annjurek@pg.edu.pl; Tel.: +48-58-347-2352

Received: 20 October 2019; Accepted: 5 November 2019; Published: 8 November 2019

Abstract: Different TiO_2 photocatalysts, i.e., commercial samples (ST-01 and P25 with minority of rutile phase), nanotubes, well-crystallized faceted particles of decahedral shape and mesoporous spheres, were used as supports for deposition of Pt nanoparticles (NPs). Size-controlled Pt NPs embedded in TiO_2 were successfully prepared by microemulsion and wet-impregnation methods. Obtained photocatalysts were characterized using XRD, TEM, X-ray photoelectron spectroscopy (XPS), Brunauer–Emmett–Teller (BET) specific surface area, DR/UV-vis and action spectrum analysis. The effect of deposition method, amount of Pt precursor and TiO_2 properties on size, distribution, and chemical states of deposited Pt NPs were investigated. Finally, the correlations between the physicochemical properties and photocatalytic activities in oxidation and reduction reactions under UV and Vis light of different Pt-TiO_2 photocatalysts were discussed. It was found that, regardless of preparation method, the photoactivity mainly depended on platinum and TiO_2 morphology. In view of this, we claim that the tight control of NPs' morphology allows us to design highly active materials with enhanced photocatalytic performance. Action spectrum analysis for the most active Pt-modified TiO_2 sample showed that visible light-induced phenol oxidation is initiated by excitation of platinum surface plasmon, and photocatalytic activity analysis revealed that photoactivity depended strongly on morphology of the obtained Pt-modified TiO_2 photocatalysts.

Keywords: Pt-TiO_2; heterogeneous photocatalysis; microemulsion; platinum size; TiO_2 particle size; titania morphology

1. Introduction

The photocatalytic properties of titanium (IV) oxide are applied for degradation of emerging organic pollutants in the aqueous and gaseous phases [1–4], microorganisms [5], self-cleaning and anti-fogging surfaces [6]. Attempts have also been made to photocatalytic water splitting, photocurrent generation and photoconversion of CO_2 to various hydrocarbons in the presence of TiO_2 irradiated by artificial sources of light (UV/vis lamps), as well as under natural solar radiation [7,8].

There are two major challenges facing titania photocatalysts for common applications, i.e., (i) the ability to absorb light in a broader spectrum range (UV-vis), and (ii) inhibition of charge carrier recombination (typical for all semiconductors). Various methods have been proposed to improve performance of titania, such as surface modification, doping, coupling with other materials, as well as optimization of physicochemical properties, including particle/crystallite size, specific surface area and specific morphology of titania nanoparticles (NPs) [9–15].

Recently, there are more and more reports on preparation of metal-modified TiO_2 focusing on noble and semi-noble metal NPs. Several studies have aimed on preparation of TiO_2 responsive to visible light or with enhanced photocatalytic activity under UV irradiation [16,17]. A considerable increase of photoactivity was reported for platinum deposited on TiO_2. Platinum is one of the most active metals that facilitate charge carriers' separation [18,19]. It should be pointed that photocatalytic efficiency under UV irradiation depends strongly on the electron transfer from the excited semiconductor to metal particle deposited on its surface [20]. For example, Xiong et al. [21] deposited Pt NPs on TiO_2 using photodeposition and chemical reduction methods. They found that photodeposition using H_2PtCl_6 as a precursor contributed to smaller sizes of Pt NPs than chemical deposition using $Pt(NH_3)_4Cl_2$ as a platinum ions' source [21]. However, the mechanism of smaller Pt particles formation on TiO_2 surface with enhanced photoactivity was not investigated. On the other hand, deposition of platinum onto commercial TiO_2 P25 (Evonik) resulted in lower photocatalytic activity in phenol degradation [22].

The second approach to enhance semiconductor photoactivity is focused on the design of TiO_2 morphology and microstructure during preparation procedure in order to achieve enhanced photodegradation of persistent organic pollutants. In view of this, TiO_2 nanotubes, mesoporous and hollow spheres offer a robust template for the modification of TiO_2 surface. Both surface adsorption as well as photocatalytic reaction can be enhanced by development of surface area of TiO_2 since more reactive sites for degradation of organic compounds are available. As so far, the effect of TiO_2 morphology (particle size and shape) on the properties and distribution of platinum NPs has not been investigated in detail. Therefore, in the present work, the effect of Pt content and synthesis conditions on the preparation of Pt NPs with desired properties and enhanced photocatalytic activity under UV and visible light irradiation (λ > 400 nm) was investigated. For the first time, the correlations between physicochemical properties and photocatalytic activities of different Pt-TiO_2 photocatalysts were discussed. Size-controlled Pt NPs were obtained using a water-in-oil microemulsion or wet-impregnation method. In microemulsion, ultrafine nanoparticles with a specific diameter, morphology and narrow size distribution were obtained, since the water nanodroplets surrounded by a monolayer of surfactant in a continuous oil phase acted as microreactors to synthesize NPs of controlled growth inside the water droplet. Furthermore, commonly used the sol–gel method as a simple and inexpensive process was used for the preparation of nanoparticles and nanocomposites with a high degree of purity of the obtained products.

2. Results

2.1. Structural, Textural and Surface Characteristic of TiO_2 Photocatalysts

It is well known that surface properties of photocatalysts influence significantly the photocatalytic activity. For example, it has been proposed that the enhanced photocatalytic activity is attributed to the fast separation of photogenerated charge carriers' (such as electron transfer to {101} and hole transfer to {001} in faceted crystal), improved light absorption, high specific surface area as well as multi-porous structure of the photocatalyst. In order to obtain highly active TiO_2 photocatalysts as supports for platinum nanoparticles, anatase with: (i) well-controlled morphology (decahedral anatase particles TiO_2_DAP, Figure 1a), (ii) multi-porous structure TiO_2_NS (Figure 1b) and (iii) high specific surface area (titania nanotubes TiO_2_NT, Figure 1c) were prepared in this study. It was proposed that a porous structure provides more single sites and special passages for charge transport, which results in markedly enhanced photocatalytic activity. Whereas, titania nanotubes

with high specific surface area might also benefit from the light-matter interaction, due to the multiple scattering effect and more exposed active sites [23].

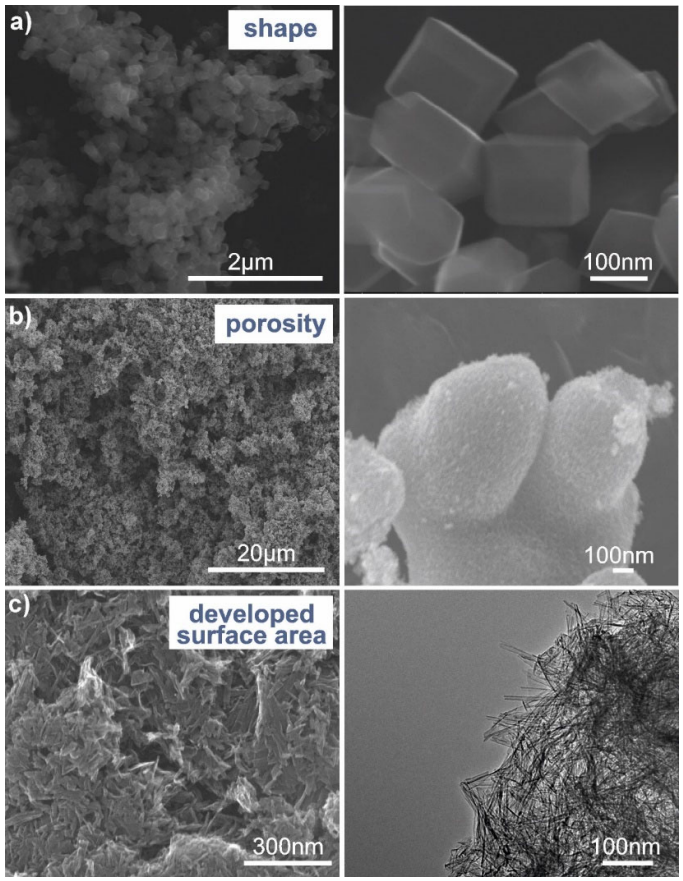

Figure 1. Microscopic images of bare decahedral anatase particles TiO_2_DAP67 (**a**), TiO_2 nanospheres TiO_2_NS (**b**) and TiO_2 nanotubes TiO_2_NT_450 calcined at 450 °C (**c**).

Indeed, three different titania nanostructures were successfully prepared, as shown in Figure 1. Decahedral anatase particles (DAP) possess the largest NPs' sizes among them in the range of 15–150 nm, as shown in Figure 1a for the TiO_2_DAP67 sample with the largest crystallites. Whereas, the smallest NPs were observed for multi-porous TiO_2 nanospheres (Figure 1b). The titania nanotubes (Figure 1c sample TiO_2_NT_450) obtained in hydrothermal reaction at 130 °C and calcined at 450 °C had an inner diameter of 5 nm, outer diameter of 8 nm and length in the range of 60 nm to 80 nm.

The properties of TiO_2 nanostructures used for deposition of platinum NPs are presented in Table 1. The crystallinity, phase composition and crystallite size were determined by X-ray diffraction (XRD). The content of amorphous phase for commercial TiO_2: P25 (13%) and ST01 (7%) were similar to that found in the literature [24,25].

Table 1. Structural properties and photocatalytic activity of TiO_2 used for deposition of Pt particles.

Sample No.	TiO_2 Source	Crystallinity (%)	Crystallite Size (nm)		BET ($m^2 \cdot g^{-1}$)	Phenol Degradation Rate ($\mu mol \cdot dm^{-3} \cdot min^{-1}$)
			a	r		
TiO_2_TIP	TIP	79	10	-	81	4.29
TiO_2_TBT	TBT	85	6	-	190	6.80
TiO_2_P25	P25	87	28	33	55	6.75
TiO_2_ST01	ST01	93	8	-	250	6.12
*TiO_2_NT_350	P25	67	11	4	375	5.79

TiO_2_NT_450	P25	77	11	2	375	5.87
TiO_2_NT_550	P25	81	13	12	210	5.82
** TiO_2_NS	TIP	81	5	-	290	5.20
*** TiO_2_DAP67	$TiCl_4$	94	67	-	16	7.82
TiO_2_DAP55	$TiCl_4$	n.a.	55	-	20	6.43
TiO_2_DAP10	$TiCl_4$	n.a.	10	-	180	6.33

* TiO_2_NT—titania nanotubes obtained by hydrothermal treatment at 110 °C and calcined in temperatures 350 °C, 450 °C and 550 °C; ** TiO_2_NS—titania mesoporous spheres obtained by titanium isopropoxide (TIP) hydrolysis in the presence of ammonium citrate; *** TiO_2_DAP—decahedral anatase particles (DAPs) obtained by titanium (IV) chloride ($TiCl_4$) hydrolysis with crystallite size of 67 nm, 55 nm and 10 nm determined by XRD analysis.

Fine anatase crystallites were formed during hydrolysis of titanium isopropoxide (TiO_2_TIP) and titanium butoxide (TiO_2_TBT) of ca. 10 nm and 6 nm, respectively, and the samples were composed of anatase (ca. 80% and 85% for TiO_2_TIP and 85% for TiO_2_TBT, respectively), brookite (ca. 5%) and amorphous phase (without rutile). The crystallite sizes of TiO_2 nanotubes increased with an increase in calcination temperature from 350 °C to 550 °C. The highest crystallinity (94%) was observed for DAPs (TiO_2_DAP67), which is not surprising and typical for faceted samples. The crystallite sizes of DAPs increased with an increase in concentration of $TiCl_4$ in the gas mixture during the preparation procedure.

Comparing the textural properties of prepared TiO_2 photocatalysts, it can be concluded that, the sol–gel (TiO_2_TIP and TiO_2_TBT) and hydrothermal (NT) methods allow to obtain TiO_2 with developed surface areas. Moreover, the specific surface area of TiO_2_TIP is lower than that of TiO_2_TBT and TiO_2_NS, and almost all (except DAPs) prepared photocatalysts revealed larger specific surface areas than that of P25. Generally, TiO_2 with high specific surface area tends to have higher photocatalytic activity especially in the gas phase reaction, because the larger surface area facilitates more adsorption of reaction substrates and as a result the improved productivity of reactive oxygen species occurs [9]. However, in this study there is no clear relationship between the specific surface area and photocatalytic activity in reaction of phenol degradation in the aqueous phase. The highest photocatalytic activity revealed well-defined DAPs with crystallite size of 67 nm and Brunauer–Emmett–Teller (BET) surface area of 16 $m^2 \cdot g^{-1}$ (TiO_2_DAP67). However, it should be pointed that DAPs are the most active anatase titania samples, probably due to efficient charge carriers' separation. Moreover, the presence of small content of mixed-phases (e.g., anatase-rutile and anatase-brookite) might decrease the charge carriers' recombination [26,27]. Therefore, it was suggested that TiO_2 P25 (a mixture of anatase (70%–80%), rutile (20%–30%) and amorphous titania (1%–10%) exhibited high photocatalytic activity, due to possible charge transfer between phases. The obtained in this study anatase-based photocatalysts (TiO_2_TIP and TiO_2_TBT samples shown in Table 1), which contain slight content of brookite (5%) exhibited also high photoactivity. Furthermore, decahedral anatase particles (TiO_2_DAP), which possesses small content of rutile (3%) also revealed improved efficiency of phenol degradation.

In view of this, to obtain highly active under UV-vis radiation photocatalysts and to clarify the crucial parameters of photocatalytic activity under vis irradiation, anatase particles with well-defined morphology (DAPs), spherical particles of anatase with minor amount of brookite or rutile and TiO_2 nanotubes calcined at 450 °C, highly active in reaction of phenol degradation, were further used as supports for platinum nanoparticles.

2.2. Morphology of Pt-TiO_2 Photocatalysts Obtained by the Wet-Impregnation and Microemulsion Method (Me)

Sample labeling, selected properties of two Pt-TiO_2 photocatalyst series, including the type of TiO_2 source and reducing agent, amount of platinum ions used for deposition on TiO_2, average crystallite size of Pt and TiO_2, and photocatalytic properties of Pt-TiO_2 nanocomposites are listed in Table 2.

Table 2. Characteristics of Pt-modified TiO_2 obtained by wet-impregnation method.

Photocatalyst	TiO_2 Source	Amount of Platinum Precursor	Reducing Agent	Crystallite Size (nm)			Phenol Degradation Rate ($\mu mol \cdot dm^{-3} \cdot min^{-1}$)	
				Anatase (101)	Rutile (110)	Pt (111)	Under UV-Vis	Under Vis $\lambda > 420$ nm
0.05Pt-TiO_2_TIP	TIP	0.05	temperature	7	-	3	4.95	5.13
0.1Pt-TiO_2_TIP	TIP	0.1	temperature	8	-	2	5.25	5.74
0.5Pt-TiO_2_TIP	TIP	0.5	temperature	8	-	5	4.97	3.84
0.1Pt-TiO_2_P25	P25	0.1	temperature	21.5	29	5	6.18	3.15
0.1Pt-TiO_2_P25_red	P25	0.1	$NaBH_4$	20	33	6	6.20	3.10
0.1Pt-TiO_2_ST01	ST01	0.1	temperature	10	-	2	5.13	6.89
0.1Pt-TiO_2_ST01_red	ST01	0.1	$NaBH_4$	14	-	3	5.90	6.62
0.1Pt-TiO_2_DAP67	DAP *	0.1	temperature	72	-	9	7.10	3.14
0.1Pt-TiO_2_DAP67_red	DAP *	0.1	$NaBH_4$	72	-	17	7.20	2.90
0.1Pt-TiO_2_NS_red	sphere	0.1	$NaBH_4$	28		5.5	6.20	3.83

* TiO_2_DAP—decahedral anatase particles (DAPs) obtained by titanium (IV) chloride ($TiCl_4$) hydrolysis with crystallite size of 67 nm determined by XRD analysis.

The morphology of Pt-TiO_2 particles obtained by the wet-impregnation method was studied by STEM and HR-TEM, and exemplary images are shown in Figures 2 and 3. The platinum nanoparticles were deposited on ST01, TiO_2 from TIP hydrolysis and DAPs by reduction of platinum ions using thermal treatment at temperature of 400 °C. The average platinum NPs' size deposited on DAPs, obtained by thermal reduction (Figure 2a) and chemical reduction (Figure 2b), was calculated from the statistical average size distribution of 100 Pt NPs. The monodisperse distribution of Pt NPs with an average size of 7 nm and bimodal size distribution with average sizes of 7 nm and 14 nm were obtained by thermal treatment and chemical reduction, respectively, on DAPs with an average TiO_2 particle size of 105 nm. This correlation between chemical and thermal reduction was also observed for Pt NPs deposited on commercial TiO_2 P25 and ST01 surfaces, as shown in Table 2.

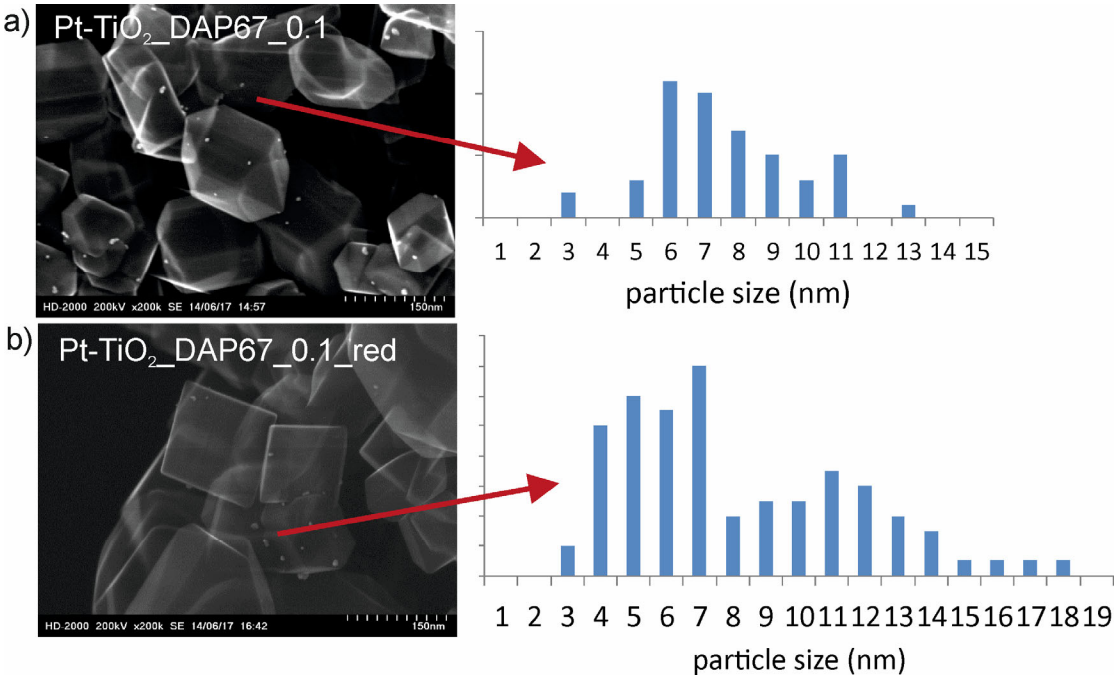

Figure 2. Microscopy images of decahedral anatase particles modified with Pt and platinum size distribution for 0.1Pt-TiO_2_DAP67 obtained by thermal reduction (**a**) and 0.1Pt-TiO_2_DAP67_red obtained by chemical reduction of platinum ions on DAPs' surface (**b**).

The average crystallite sizes of Pt deposited on TiO_2 P25 and ST01 using sodium borohydride as a reducing agent were larger than crystallite sizes of Pt deposited on the same TiO_2 during thermal treatment. The microscopy analysis (TEM) have also confirmed deposition of fine platinum nanoparticles with an average size of about 3 nm on the surface of TiO_2 ST01 and TiO_2 from TIP hydrolysis as shown in Figure 3a,b.

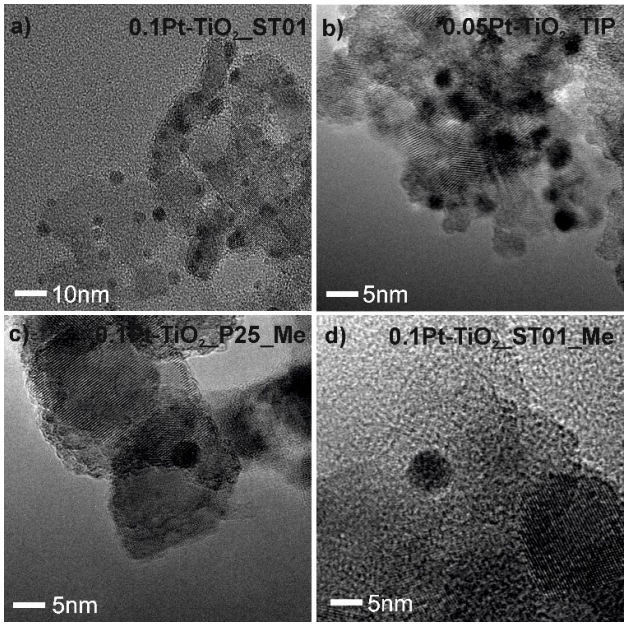

Figure 3. Microscopy images (TEM) of platinum particles deposited using the wet-impregnation method on ST01 (**a**), TiO_2 from titanium isopropoxide hydrolysis (**b**) and obtained in w/o microemulsion by deposition of Pt nanoparticles on P25 (**c**) and ST01 TiO_2 support (**d**).

Exemplary images of size-controlled Pt nanoparticles deposited on TiO_2 P25 and ST01 prepared by microemulsion method are presented in Figure 3c,d. The average Pt NPs' size, obtained in microemulsion system, was 5–6 nm, and did not depend on TiO_2 support in contrast to the wet-impregnation method. In microemulsion, aqueous phase nanodroplets containing chemical reagents are dispersed in the continuous oil phase and protected against agglomeration by surfactant at the water-in-oil interface. The water pool volume determines the maximum size of the particles, which may interchange during the growth or aggregation step of the synthesis.

The average size of the surfactant (TX-100) package micelles, estimated by DLS, was 5 nm in the range of 3–8 nm. The Pt average NPs' size of ca. 5.7 nm (see in Figure 4), which was determined by the Ostwald ripening and growth inside the water pools of reversed micelles, correlates well with micelles' size, and corresponds to the 5–6 nm mean particle diameter in TEM images (Figure 3c,d) and crystallite size of Pt (111) calculated based on Scherrer formula. Summarized crystallographic data with photocatalytic properties of Pt-modified TiO_2 samples obtained in w/o microemulsion are shown in Table 3. For platinum NPs obtained in w/o microemulsion with addition of 25% HCl smaller cubic nanoparticles (sample 0.1Pt-TiO_2_ST01_Me_3) with crystallite size of 3 nm were obtained.

The interaction between the ionic species (Cl^- ions) and platinum results in stabilization of fine particles in microemulsion system. Similarly, Kitchens et al. found that addition of HCl to the compressed propane reverse micelle system affected the properties of formed copper NPs. Moreover, addition of chloride ions led to the formation of stable diamond shaped assemblies [28].

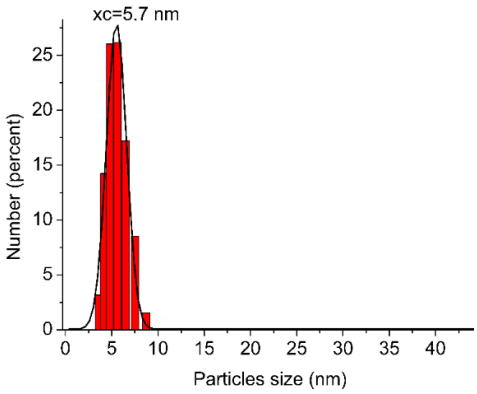

Figure 4. Platinum particles size distribution obtained by reduction of platinum ions in water cores using sodium borohydride in the water-TX100-cyclohexane microemulsion system.

Table 3. Characteristics of Pt-modified TiO_2 obtained by the microemulsion method.

Photocatalyst	TiO_2 Source	Crystallite Size (nm)			Phenol Degradation Rate ($\mu mol \cdot dm^{-3} \cdot min^{-1}$)	
		Anatase (101)	Rutile (110)	Pt (111)	Under UV-Vis	Under Vis $\lambda > 420$ nm
0.1Pt-TiO_2_ST01_Me_1	ST01	12	-	6	7.49	4.09
0.1Pt-TiO_2_ST01_Me_2	ST01	13	-	4	7.46	5.04
*0.1Pt-TiO_2_ST01_Me_3	ST01	13	-	3	7.52	6.62
0.1Pt-TiO_2_P25_Me_4	P25	20	29	5	7.50	3.15
0.1Pt-TiO_2_DAP67_Me_5	DAP67	91	158	5	7.52	3.63
0.1Pt-TiO_2_NT110_Me_6	NT110	15	-	6.5	6.77	2.41

* Pt-TiO_2_Me_3 - cubic platinum nanoparticles obtained in w/o microemulsion containing 25% HCl.

The TiO_2 crystal structure and platinum crystal system was evaluated using the XRD analysis (shown in Figure 5). The 0.1Pt-TiO_2_P25, 0.1Pt-TiO_2_P25_red and 0.1Pt-TiO_2_P25_Me_4 samples as expected were mainly composed of anatase (89%) and rutile (11%; Figure 5a). The typical diffraction peaks corresponding to anatase were observed at $2\theta = 25°$, 38°, 38.5°, 48°, 54°, 62°, 70° and 75° (JCPDS card No. 89-4203). The reflections attributed to rutile were indexed at $2\theta = 27°$, 36°, 41°, 44°, 54°, 56.6° and 76.7° (JCPDS, No. 76-1940). The most intense diffraction peaks of 0.1Pt-TiO_2_ST01, 0.1Pt-TiO_2_ST01_Me_1 and 0.1Pt-TiO_2_ST01_Me_3 photocatalysts in the XRD patterns (Figure 5b) at 25°, 38°, 48°, 54°, 62.7°, 70°, 75° and 83° can be attributed to (101), (103), (200), (105), (213), (116), (107) and (303) reflections of anatase TiO_2.

Although, the most intense diffraction peaks of fine Pt particles overlapped with anatase (103) and (200) plane in the XRD pattern, the analysis allowed to estimate the crystallite sizes of Pt NPs based on Scherrer equation. For Pt-TiO_2_Z9 and Pt-TiO_2_Me_6 the diffraction peaks at 39.8° and 46° could be attributed to platinum (111) and (200) plane deposited on decahedral anatase particles and TiO_2 nanotubes (see in Figure 5d).

The chemical composition of Pt-TiO_2 samples was estimated by X-ray photoelectron spectroscopy (XPS) analysis, and the obtained data are presented in Table 4 and Figures 6 and 7. Considering chemical state of titanium, all the samples consisted mainly of Ti^{4+}, and the content of Ti^{3+} reached only ca. 0.6% and 1.6% for 0.1Pt-TiO_2_P25_Me_4 and 0.1Pt-TiO_2_ST01, respectively (see in Table 4). A slight increase in the content of Ti^{3+} was observed for platinum deposited on ST01 anatase particles. Moreover, ST01 modified with Pt exhibited higher O/Ti ratio compared to P25 and DAPs decorated with platinum. Based on density functional theory slab calculations Han et al. [29] stated that higher concentration of oxygen vacancies on TiO_2 surface is the crucial parameter that controls the growth of metallic particles on TiO_2. In view of this, in the present study smaller TiO_2 particles, which possess higher density of oxygen traps and nucleation sites resulted in deposition of smaller platinum particles on the TiO_2 surface (e.g., ST-01) compared to DAPs and TiO_2 nanotubes.

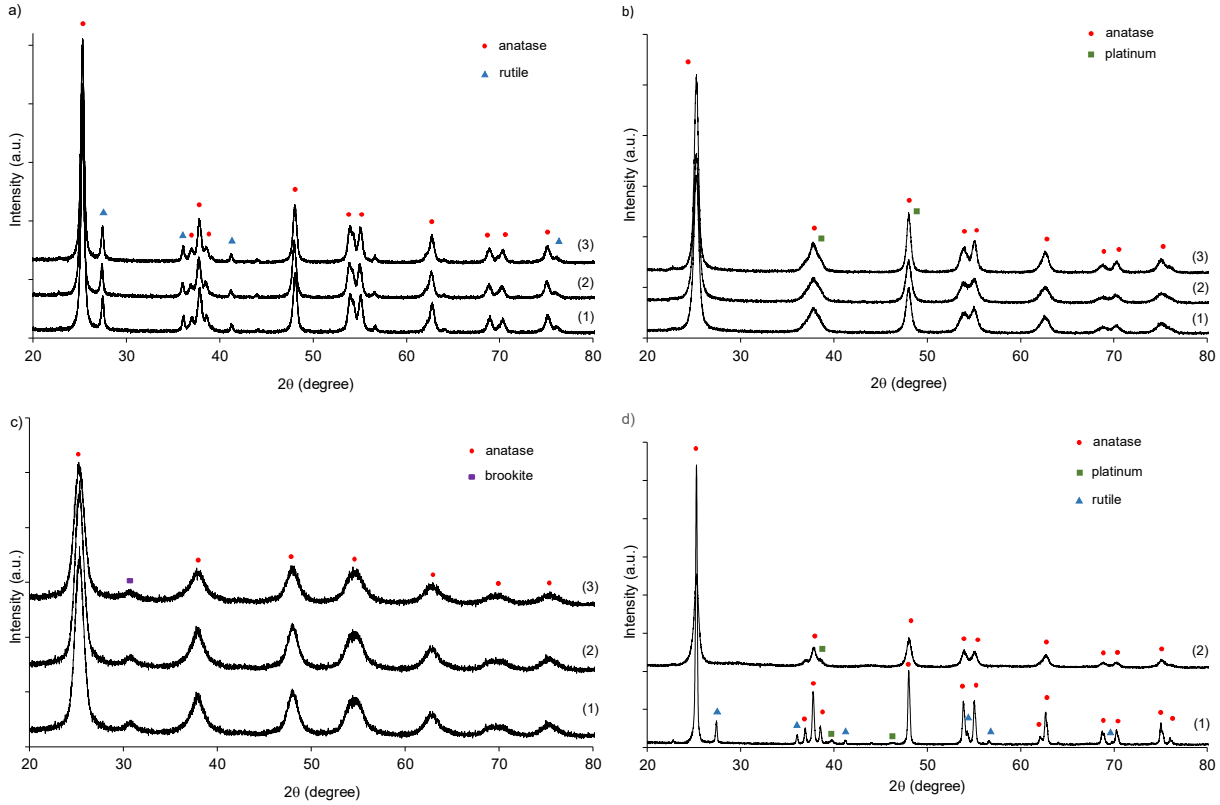

Figure 5. XRD patterns of (1) 0.1Pt-TiO_2_P25, (2) 0.1Pt-TiO_2_P25_red and (3) 0.1Pt-TiO_2_P25_Me_4 samples with marked anatase and rutile peaks (**a**); (1) 0.1Pt-TiO_2_ST01, (2) 0.1Pt-TiO_2_ST01_Me_1 and (3) 0.1Pt-TiO_2_ST01_Me_3 with anatase and platinum signals (**b**); (1) 0.1Pt-TiO_2_NS_red, (2) 0.1Pt-TiO_2_TIP and (3) 0.5Pt-TiO_2_TIP anatase (**c**) and (1) 0.1Pt-TiO_2_DAP67_red and (2) 0.1Pt-TiO_2_NT110_Me_6 with marked anatase, platinum and rutile peaks (**d**).

Table 4. Fraction of oxidation states of Ti and surface composition of various samples of Pt-modified TiO_2 determined by X-ray photoelectron spectroscopy (XPS) analysis.

Sample Labeling	TiO_2 Source	Ti $2p_{3/2}$ (%)		Content (at.%)			Ratio
		Ti^{4+}	Ti^{3+}	Ti	O	Pt	O/Ti
0.1Pt-TiO_2_ST01	ST01	98.4	1.6	12.8	87.0	0.2	6.8
0.1Pt-TiO_2_ST01_Me_3	ST01	98.6	1.4	13.3	87.6	0.1	6.5
0.1Pt-TiO_2_P25_Me_4	P25	99.4	0.6	20.7	79.1	0.2	3.8
0.1Pt-TiO_2_DAP67	DAP	99.1	0.9	26.7	73.0	0.3	2.7
0.1Pt-TiO_2_DAP67_Me_5	DAP	99.0	1.0	27.9	71.7	0.4	2.6

The O 1s XPS spectra in Figure 6 can be resolved into three peaks, which are ascribed to (1) the lattice oxygen, (2) Ti_2O_3 and –OH groups bound to two titanium atoms and (3) hydroxyl groups bound to titanium at 529.53 eV, 531.79 eV and 533.32 eV, respectively.

For decahedral anatase particles significant increase in the content of lattice oxygen and a decrease in the content of hydroxyl oxygen was observed, suggesting that platinum nanoparticles mainly replaced hydroxyl groups adsorbed on the surface of DAPs. Regarding the heterogeneous nucleation mechanism this resulted in larger platinum particles deposited on the TiO_2 DAPs surface compared to ST01 and P25 TiO_2 support. The Pt 4f XPS spectra in Figure 7 showed that Pt existed as Pt(0), Pt(II) and Pt(IV) in all samples. The ratios of Pt(0)/Pt(σ+) were calculated based on the areas of the XPS peaks. The results revealed that samples prepared by thermal reduction of Pt ions possess much lower Pt(0)/Pt(σ+) ratios than those by microemulsion method with chemical reduction of platinum precursor using sodium borohydride. For 0.1Pt-TiO_2_ST01_Me_3 and 0.1Pt-TiO_2_DAP67_Me_5, the ratio of Pt(0) to Pt(σ+) was 40:60 and 30:70, respectively. However, it should

be pointed that XPS analysis gave only information for the surface composition, and thus it was proposed (based also on XRD data) that the metallic core of Pt was covered with platinum ions layer.

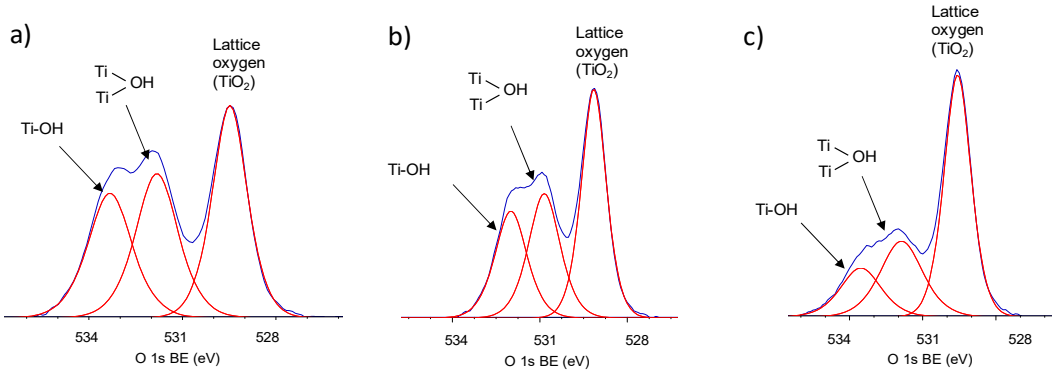

Figure 6. XPS results for O 1s for the most active 0.1Pt-TiO_2_ST01 (**a**), 0.1Pt-TiO_2_ST01_Me_3 (**b**) and 0.1Pt-TiO_2_DAP67_Me_5 (**c**) samples.

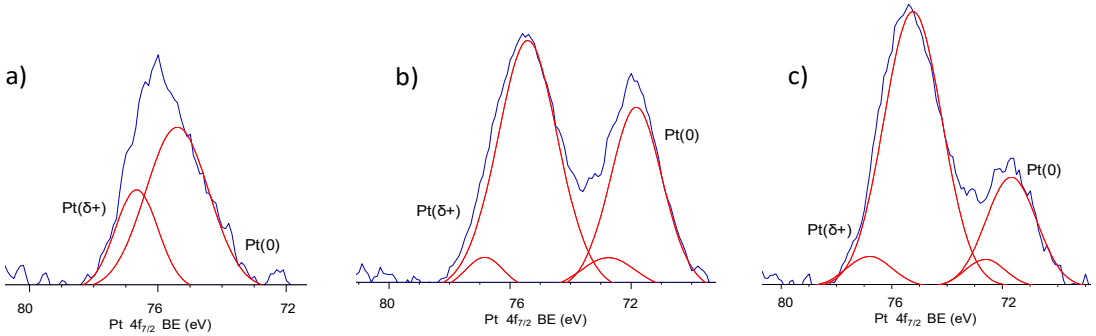

Figure 7. Pt 4f spectra for 0.1Pt-TiO_2_ST01 (**a**), 0.1Pt-TiO_2_ST01_Me_3 (**b**) and 0.1Pt-TiO_2_DAP67_Me_5 (**c**) samples.

Exemplary DR/UV-Vis spectra of Pt-TiO_2 samples are presented in Figure 8. The intrinsic interband absorption of titania was observed at wavelengths shorter than 400 nm. For Pt-modified TiO_2 nanocomposites, broad absorption band in the range from 400 nm to 800 nm was observed. The main localized surface plasmon resonance (LSPR) peak was found at 410 nm. An increase of absorption in the visible-near infrared region resulted from tailoring of platinum LSPR and/or electron transport from Pt^{II} to Pt^{IV} species [5,30–32]. The highest absorption band was observed for 0.1Pt-TiO_2_ST01 and 0.1Pt-TiO_2_ST01_Me_3 containing small spherical nanoparticles of platinum deposited on commercial TiO_2 ST01.

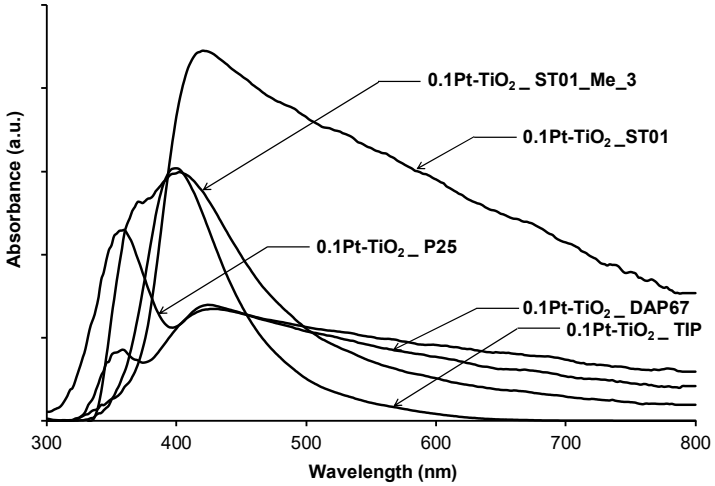

Figure 8. DR/UV-vis spectra of platinum-modified TiO_2 samples taken with bare TiO_2 supports as a reference.

2.3. Photocatalytic Activity and Property-Activity Correlations for Pt-TiO_2 Samples

Kinetics of phenol photodegradation in aqueous solution under UV-vis and visible light irradiation in the presence of Pt-modified TiO_2 nanoparticles is shown in Figure 9 and the observed rate constants are also listed in Tables 2 and 3. The best photocatalytic activity under UV-vis light showed well crystallized decahedral anatase particles decorated with larger Pt NPs and obtained using the wet-impregnation method, see in Figure 9a. Among Pt-TiO_2 samples prepared in microemulsion the photoactivity under UV-vis was comparable to the efficiency of phenol degradation for commercial TiO_2 ST01 and P25 (Figure 9b). The enhanced phenol photooxidation for all the Pt-TiO_2 samples was observed under vis light irradiation. The photocatalytic activity increased from 2.90 $\mu mol \cdot dm^{-3} \cdot min^{-1}$ to 6.89 $\mu mol \cdot dm^{-3} \cdot min^{-1}$ for 0.1Pt-TiO_2_DAP67_red and 0.1Pt-TiO_2_ST01, respectively. An increase of platinum content above 0.1 mol% resulted in a decrease of phenol degradation rate for 0.05Pt-TiO_2_TIP (0.05 mol% Pt), 0.1Pt-TiO_2_TIP (0.1 mol% Pt) and 0.5Pt-TiO_2_TIP (0.5 mol% Pt) caused by increase of crystallite size from 2–3 nm (0.05 mol% Pt) to 5 nm (0.5 mol% Pt). Moreover, higher photoactivity revealed photocatalysts modified with Pt obtained by thermal reduction of platinum ions on the surface of P25, ST01 and DAPs (see samples 0.1Pt-TiO_2_P25, 0.1Pt-TiO_2_ST01 and 0.1Pt-TiO_2_DAP67) compared to chemical reduced platinum ions using sodium borohydride (samples 0.1Pt-TiO_2_P25_red, 0.1Pt-TiO_2_ST01_red and 0.1Pt-TiO_2_DAP67_red).

The obtained results clearly indicated that the photocatalytic activity mainly depended on platinum particles size. In a microemulsion system platinum particles size is controlled by size of reverse micelles and addition of ions (e.g., Cl^-), which affects properties of double electrical layer and as a result platinum particles growth. Most of Pt-TiO_2 samples obtained in microemulsion revealed similar particles size and photocatalytic activity. The 0.1Pt-TiO_2_ST01_Me_1 sample was obtained by deposition of platinum colloidal particles on ST01, while for 0.1Pt-TiO_2_ST01_Me_2 platinum ions dispersed in water cores of microemulsion were reduced on ST01 surface by adding microemulsion containing reducing agent in water cores.

The lower Pt particles size for 0.1Pt-TiO_2_ST01_Me_2 and 0.1Pt-TiO_2_ST01_Me_3 (obtained by adding 25% HCl into microemulsion system before reduction of Pt ions) resulted in higher photoactivity compared to 0.1Pt-TiO_2_ST01_Me_1. Therefore, interaction between metal-TiO_2 formed at the interface before reduction of transition metal ions is important for the preparation of fine Pt particles. As presented in Figure 9c,d, the best photocatalytic activity in phenol oxidation revealed samples containing platinum particles with diameter of about 2–3 nm deposited on TiO_2 almost regardless of the preparation method (wet-impregnation or microemulsion) or Pt particles shape (spherical or cubic). The highest phenol degradation rate exhibited 0.1Pt-TiO_2_ST01, 0.1Pt-TiO_2_ST01_red, 0.1Pt-TiO_2_ST01_Me_3 and 0.1Pt-TiO_2_TIP containing fine platinum particles

deposited on TiO_2 support (ST01, TIP). For that the samples phenol degradation rate was 6.89 $\mu mol \cdot dm^{-3} \cdot min^{-1}$, 6.62 $\mu mol \cdot dm^{-3} \cdot min^{-1}$ and 5.74 $\mu mol \cdot dm^{-3} \cdot min^{-1}$, respectively. Particles with a diameter above 5–6 nm exhibited significantly lower photocatalytic activity. For 0.1Pt-TiO_2_P25_red and 0.1Pt-TiO_2_P25_Me_4 containing Pt particles (5–6 nm) deposited on P25 the efficiency of phenol degradation was about 3.15 $\mu mol \cdot dm^{-3} \cdot min^{-1}$, see in Figure 9d. The results suggest that TiO_2 support type is important for the nucleation and growth of platinum particles (Figure 9e). For Pt-TiO_2 prepared using the same TiO_2 template, platinum particle size and obtained phenol degradation rates were similar. In the wet-impregnation method, larger Pt particles were formed on larger TiO_2 support particles and therefore lower photocatalytic activity in reaction of phenol oxidation for DAP, TiO_2 nanotubes and nanospheres under Vis light were observed.

The hydrogen generation analysis performed for the most active 0.1Pt-TiO_2_ST01 and Pt-TiO_2_ST01_red photocatalysts indicated that under UV light higher photoactivity revealed sample containing larger platinum particles deposited on ST01 (0.1Pt-TiO_2_ST01_red) than sample containing fine Pt (2–3 nm) particles deposited on the same support (sample 0.1Pt-TiO_2_ST01). The rate of hydrogen generation was 6.82 $\mu mol \cdot g^{-1}$ for 0.1Pt-TiO_2_ST01_red and 5.93 $\mu mol \cdot g^{-1}$ for 0.1Pt-TiO_2_ST01.

For the most active Pt-modified ST01 sample the action spectrum analysis was performed, and the results are presented in Figure 9f. Action spectrum analysis is a wavelength dependence of apparent quantum efficiency, and the photoabsorption spectrum, which confirm that a nanomaterial works as a photocatalyst [32]. The 0.1Pt-TiO_2_ST01 gave action spectrum that resembled respective absorption spectrum measured in a diffuse reflection mode using $BaSO_4$ as a reference material.

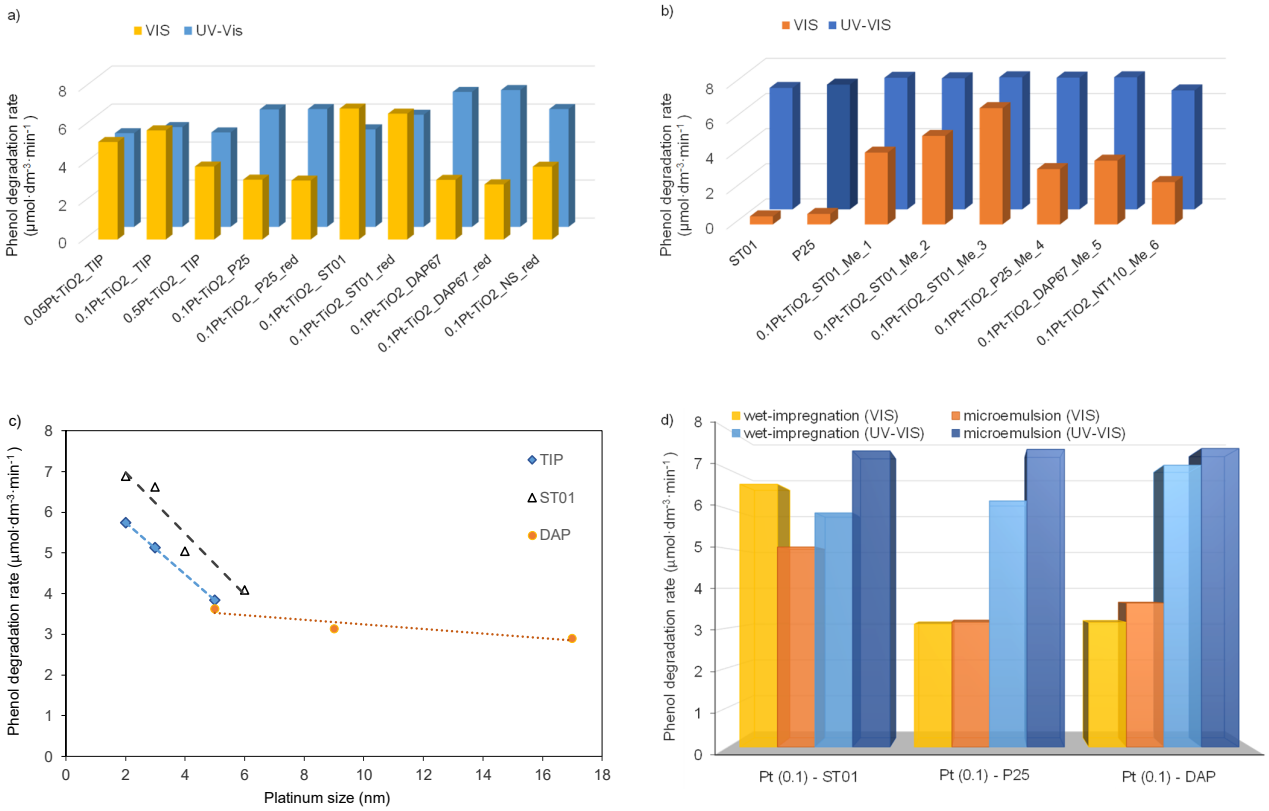

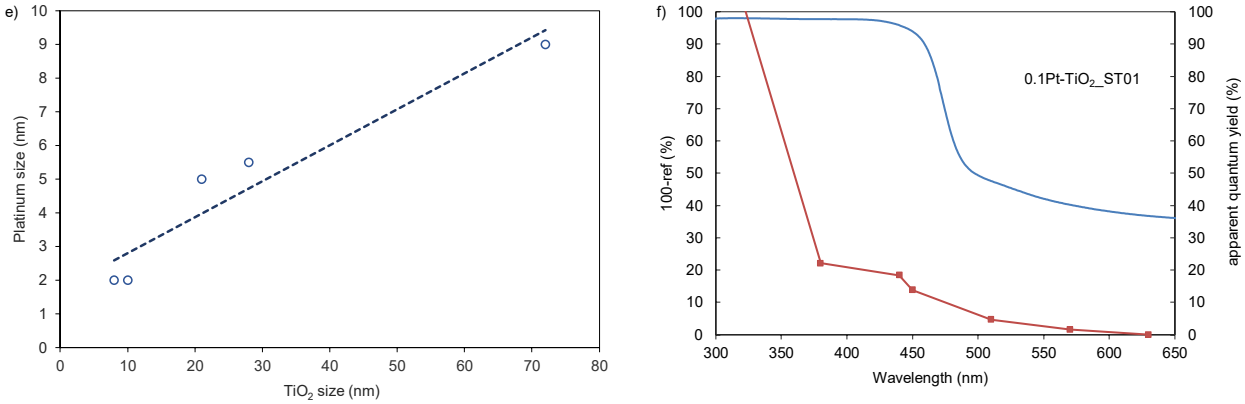

Figure 9. Photocatalytic activity for Pt-TiO_2 samples obtained by the wet-impregnation method (**a**), Pt-TiO_2_Me samples obtained in w/o microemulsion system (**b**), Correlation between platinum particle size and photocatalytic activity of TIP, ST01 and DAP (**c**), Comparison of UV-vis and visible-light photocatalytic activity of Pt-modified samples based on ST01, P25 and DAP titania particles obtained using wet-impregnation and microemulsion methods (**d**), Correlation between platinum particle size and TiO_2 support particle size (**e**) and action spectrum of phenol oxidation on 0.1Pt-TiO_2_ST01 (**f**).

The action spectrum correlated with the absorption spectrum at the wavelength range from 365 nm to 440 nm, associated with TiO_2 and Pt plasmonic excitation, respectively. In view of this, under UV light the mechanism of photocatalytic activity was attributed to the charge carriers' separation enhanced by electronic interaction occurring at the contact region between metal deposits and semiconductor surface leading to removal of electrons from TiO_2 ST01 into Pt nanoparticles. Further, under vis light, localized surface plasmon resonance (LSPR) of Pt NPs was beneficial for light absorption. Therefore, enhanced photocatalytic activity was observed during irradiation ($400 > \lambda > 450$ nm) of fine Pt particles deposited on TiO_2 support.

3. Discussion

Highly active commercial anatase ST01, standard material (P25) consisting of a mixture of anatase and rutile particles, well-crystallized anatase decahedral particles, TiO_2 nanospheres and nanotubes with developed surface area were used as templates for Pt particles formation.

Pt-modified photocatalysts revealed either enhanced or reduced UV-vis and visible light activity, depending on morphology of platinum NPs and host titania. The interaction between metal-TiO_2 formed at the interface before reduction of transition metal ions was crucial for the preparation of Pt particles with defined morphology by the wet-impregnation method.

Based on the obtained results, the schematic mechanism of Pt particles deposition on TiO_2 with different morphological properties was proposed and presented in Figure 10. Generally, surface defects such as oxygen vacancies plays an important role in heterogeneous nucleation mechanism of transition metal growth on semiconductor surface. For decahedral anatase particles, the reduced TiO_2 {101} surface is electron-rich, whereas the oxidized TiO_2 {001} is electron-deficient. Therefore, Pt adatoms deposited preferably on oxygen vacancy sites on the anatase TiO_2 {101} surface. Moreover, as shown in Figure 10a, electrons located on the oxygen vacancy states were released and the adsorbed Pt ions were reduced. After thermal treatment, the colloidal species grown by cluster mobility and Ostwald ripening on the surface of DAPs TiO_2. In the chemical reduction method, a solution-dominated reduction pathway promoted seed-mediated growth mechanism of Pt species on TiO_2 surface. The surface of the seeds simultaneously acts as both deposition and reduction site, facilitating further growth of Pt and resulting in larger Pt NPs deposition on TiO_2. Furthermore, this behavior can be explained by the fact that in sodium borohydride environment during chemical reduction, TiO_2 surface is partially reduced and has very few nucleation sites for Pt deposition compared to the oxidized surface of TiO_2 during thermal treatment.

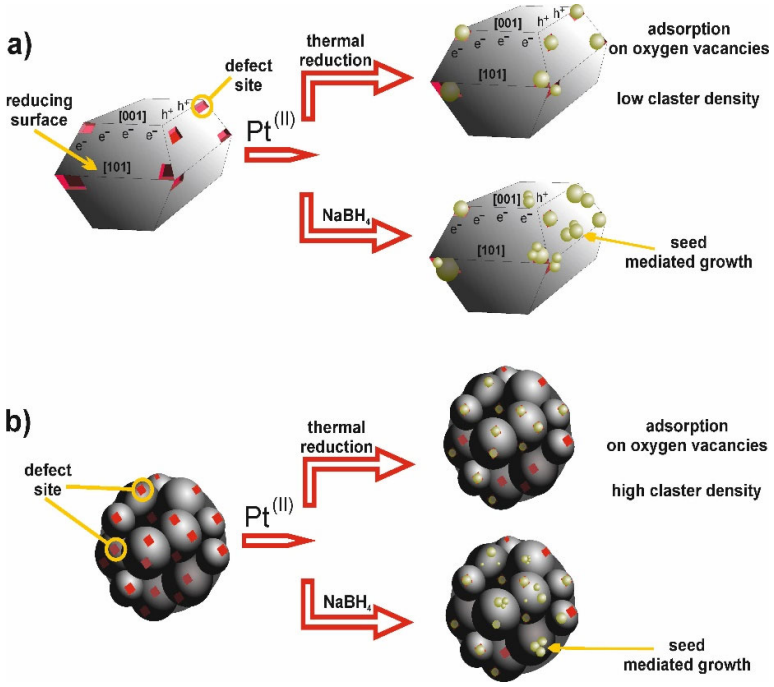

Figure 10. Schematic illustration of the proposed mechanism of Pt particles deposition on decahedral anatase particles (**a**) and spherical particles with developed surface area and nucleation sites for controlled particle growth (**b**).

The XPS results confirmed that samples prepared by thermal reduction of Pt ions possess much lower Pt(0)/Pt(σ+) ratios than those by chemical reduction of platinum precursor using sodium borohydride. Moreover, for decahedral anatase particles an increase in the content of lattice oxygen and a decrease in the content of hydroxyl oxygen was observed, suggesting that platinum nanoparticles mainly replaced hydroxyl groups adsorbed on the surface of DAPs. Regarding the heterogeneous nucleation mechanism this resulted in larger platinum particles deposition on the TiO_2 DAPs surface compared to ST01 and P25 TiO_2 support. The surface of ST01 modified with Pt exhibited higher O/Ti ratio and content of Ti^{3+} compared to P25 and DAPs decorated with platinum. Therefore, smaller TiO_2 particles with higher density of oxygen traps and nucleation sites resulted in deposition of smaller platinum particles on the ST01 surface compared to DAPs, as shown in Figure 10b. XRD and TEM analysis corroborate that higher photoactivity under Vis revealed photocatalysts containing Pt with particle size below 3 nm obtained by thermal reduction of platinum ions on the surface of ST01 and DAPs than during chemical reduction using sodium borohydride**.** At the same time, under UV light higher photoactivity in phenol photooxidation as well as hydrogen evolution reactions revealed samples containing larger platinum particles deposited on TiO_2 template.

The results obtained are consistent with literature reports. The rate of diffusion and corresponding Pt particle size can be predicted based on the metal–titania and admetal–oxygen binding energies. Galhenage et al. [33] confirmed that the metal–titania adsorption energies are higher on the oxidized surfaces, and this is consistent with the lower diffusion rates resulting in smaller metal particles sizes and higher cluster densities compared to the growth on reduced TiO_2 [33]. Furthermore, Campbell et al. [34] reported that for metal deposition on alumina, silica and zirconia, the adhesion energies correlate with negative free energy of formation. In this regard, the adhesion energies are related to strength of local chemical bonds formed at metal–oxygen and metal–metal interface [34].

Summarizing, for deposition of metal particles on TiO_2 support without using surfactants, the corresponding particle sizes mainly are determined by Pt-TiO_2 and Pt-O-TiO_2 interactions and the presence of nucleation sites that attract metal adatoms diffusing on the surface of metal oxide particle. In microemulsion obtained metal particles were protected and stabilized against agglomeration by

the surfactant at the interface of water-in-oil. That allowed us to obtain size-controlled Pt particles (6–7 nm) embedded in TiO_2.

4. Materials and Methods

4.1. Preparation of TiO_2 and Pt-TiO_2 Photocatalysts

All the reagents used in experiments were of analytical grade (purchased from Aldrich, Saint. Louis, MO, USA). Three kinds of decahedral anatase particles (DAPs), samples with different crystal sizes, were prepared from titanium (IV) chloride ($TiCl_4$) and oxygen by rapid heating (1373 K) and quenching of gas reaction mixture [10].

Titania nanotubes (NT) were obtained by mixing appropriate amount of TiO_2 nanoparticles (P25) with 10 M NaOH solution. After 1-h of stirring, the suspension was transferred to a Teflon-lined stainless-steel autoclave (200 cm^3) and heated at 110 °C for 12 h. After hydrothermal reaction, the autoclave was allowed to cool to room temperature, and the final product was filtered and washed with 0.1 M HCl and distilled water, until the pH value of the washing solution was lower than 7. Subsequently, the obtained NT were dried at 80 °C and calcinated at 350–650 °C.

In a preparation of mesoporous TiO_2 spheres (sample labeled as TiO_2_NS), 3 mM solution of citric acid in 3 cm^3 of water was added to 60 cm^3 of ethanol. After the solution was stirred, 20 cm^3 of ammonium hydroxide and 10 cm^3 of titanium (IV) butoxide (Fluka, 99%) were added dropwise at the same time. The rate of ammonia addition was two times faster than that of TiO_2 precursor. After 6-h of stirring, the suspension was centrifuged (2000 rpm for 5 min), washed with distilled water, dried at 50 °C to constant mass and calcinated at 400 °C for 2 h.

Anatase nanoparticles were prepared by hydrolysis of titanium (IV) isopropoxide (TIP) or titanium (IV) butoxide (TBT). In this regard, TIP or TBT was added to ethanol and stirred for 15 min. Subsequently, 5.71 cm^3 of water was added to the alkoxide solution and white thick precipitate was formed. The rate of water addition was kept at 0.5 $cm^3 \cdot min^{-1}$. The molar ratio of H_2O to TiO_2 precursor (TIP or TBT) was 12. Then, the suspension was centrifuged (2000 rpm for 5 min), washed with distilled water, dried at 80 °C to constant mass, and calcinated at 400 °C for 3 h.

Such obtained TiO_2 particles, i.e., decahedral anatase particles (TiO_2_DAP), nanotubes (TiO_2_NT), mesoporous nanospheres (TiO_2_NS), titania from hydrolysis of precursors: TiO_2_TIP, TiO_2_TBT and commercial TiO_2: ST-01 anatase (particle size: 8 nm, S_{BET} = 250 $m^2 \cdot g^{-1}$, supplier: Ishihara Sangyo Ltd., Osaka, Japan), P25 (a mixture of the crystalline phases: anatase (73%–85%), rutile (14–17%) and amorphous titania (0%–13%) [14], S_{BET} = 50 $m^2 \cdot g^{-1}$ supplier: Evonik, Essen, Germany), were used for the preparation of Pt-modified TiO_2 photocatalysts.

4.2. Preparation of Pt-TiO_2 Photocatalysts

Chloroplatinic acid hexahydrate was provided by Aldrich and used as a starting material for the preparation of platinum NPs. The Pt-TiO_2 photocatalysts were obtained by the wet-impregnation method using the reducing agent (sodium borohydride) or thermal reduction during calcination process.

For the thermal reduction method, a certain amount of H_2PtCl_6 aqueous solution was added at room temperature into TiO_2 gel or suspension of commercial TiO_2 in ethanol. The obtained suspension of platinum-modified TiO_2 was centrifuged, dried at 80 °C to a dry mass and calcined at 400 °C for 2 h. Rate of heating during the calcination process was maintained at 2 °C·min^{-1}. For chemical reduction the molar ratio of the reducing agent to platinum ions equaled 3. Then sample was centrifuged, dried and calcined as described above.

In order to study the effect of platinum nanoparticles size and shape, the microemulsion method was applied for preparation of Pt-TiO_2 nanocomposites (see samples Pt-TiO_2_Me_1-Me_6). Water-in-oil microemulsion allows for tight control the shape and size of the obtained nanoparticles. The Pt-TiO_2 photocatalysts were prepared in a water-TX100-cyclohexane microemulsion. Platinum precursor solution (H_2PtCl_6) was added to 0.2 M TX-100 in cyclohexane. The water content was controlled by fixing the molar ratio of water to the surfactant at 1. Mixing of microemulsion

containing metal ions in aqueous phase was carried out for 30 min under nitrogen and then platinum was reduced by dropwise addition of the second microemulsion containing sodium borohydride as a reducing agent in aqueous phase. The molar ratio of the reducing agent to metal ions was equaled to 3. Then, titanium (IV) isopropoxide or TiO_2 (P25, ST01 or titania NT) was added into the microemulsion system containing Pt NPs. The obtained precipitate was washed with acetone and water to remove the surfactant, dried at 80 °C to constant mass and calcinated at 400 °C for 2 h.

Cubic platinum nanoparticles were obtained in water-TX100-cyclohexane microemulsion with addition of 25% HCl (sample 0.1Pt-TiO_2_ST01_Me_3). In this regard, 0.1 cm^3 25% HCl and 0.26 cm^3 of platinum precursor solution (0.048 M H_2PtCl_6) were added into 100 cm^3 of 0.2 M TX100 in cyclohexane. The Pt chemical reduction was performed by adding 50 cm^3 of water-TX100-cyclohexane microemulsion containing sodium borohydride in aqueous phase. The water content was controlled by fixing the molar ratio of water to the surfactant at 1. The concentration of the added $NaBH_4$ was 0.1875 M and $NaBH_4$ to Pt molar ratio was 3. Then, the TiO_2 ST01 was added into the microemulsion system containing cubic Pt nanoparticles. After 2 h of mixing under the nitrogen atmosphere, acetone was added into the suspension to cause phase separation. Then, obtained precipitate was washed with water and dried at 80 °C to constant mass.

Unmodified TiO_2 (from TIP hydrolysis), which was a reference material, was also prepared by the wet-impregnation and microemulsion method, but without addition of a platinum source.

4.3. Characterization of Photocatalysts

XRD analysis was performed using Rigaku Intelligent X-ray diffraction system SmartLab equipped with sealed tube X-ray generator. Data acquisition conditions were as follows: 2θ range: 20–80°, scan speed: 1°·min^{-1} and scan step: 0.01°. Scherrer equation-calculations of crystallite sizes with corrections for the instrument and strains were made by the instrument dedicated software—Rigaku PDXL (v. 2.3). The analysis of crystalline and amorphous phases was performed using an internal standard (commercial nickel oxide, Aldrich).

To evaluate the light-absorption properties of Pt-modified photocatalysts, the diffuse reflectance (DR) spectra were measured, and the data were converted to obtain the absorption spectra. The measurements were carried out on Jasco V-670 spectrophotometer (Pfungstadt, Germany) equipped with PIN-757 integrating sphere where the baseline was recorded using self-obtained TiO_2 as a reference.

Nitrogen adsorption–desorption isotherms were obtained at liquid nitrogen temperature (77 K) using Micromeritics Gemini V (model 2365) instrument (Norcross, GA, USA), and the specific surface areas were determined using the Brunauer–Emmett–Teller (BET) method.

The atomic composition was examined by X-ray photoelectron spectroscopy (XPS; JEOL JPC-9010MC with MgKα X-ray, JEOL, LTD., Tokyo, Japan) and scanning electron microscopy with energy dispersive X-ray spectroscopy (SEM/EDS, JEOL JSM-6360LA, Tokyo, Japan). For SEM/EDS measurements, average data taken from three different regions for accelerating voltage higher than 15 kV and the working distance of 10 mm were used for analyses. High-resolution transmission electron microscopic (HRTEM) images were made with FEI Europe, Tecnai F20 X-Twin transmission electron microscope.

Dynamic light scattering (DLS) analysis allowed us to determine the size distribution and polydispersity of particles. The platinum particle size measurements by DLS were performed using a Malvern Zetasizer NanoZS (Malvern Instruments Ltd., Malvern, UK).

4.4. Measurements of Photocatalytic Activity

Photocatalytic activity of Pt-TiO_2 powders under UV-vis and vis was evaluated by measuring the decomposition rate of phenol in an aqueous solution. Phenol was selected as a model pollutant since it is non-volatile, a common contaminant and frequently present in industrial wastewater. The phenol content higher than 30 mg·dm^{-3} inhibits biological treatment or even eliminates sensitive microorganisms from biological wastewater treatment process (activated sludge) and significantly

reduces the biodegradation of the other components. Therefore, the World Health Organization has limited phenol concentration in the water below 1 mg·dm^{-3}.

The suspension of photocatalyst was irradiated using a xenon lamp (6271H, Oriel, CA, USA), emitting UV-vis light. The power flux at the UV range (310–380 nm) was 30 mW·cm^{-2}. The 25 cm^3 photoreactor of 3-cm thickness of the exposure layer was equipped with a quartz window. The optical path included a water filter and a cut-off glass filter (GG 420, $\lambda > 420$ nm) for vis experiments. The temperature of aqueous phase during irradiation was kept at 20 °C using a water bath. Obtained suspension was mixed through 30 min before starting irradiation to establish the adsorption–desorption equilibrium. Aliquots of 1.0 cm^3 of the aqueous suspension were collected at regular time periods during irradiation and passed through syringe filters (Ø = 0.2 μm) to remove the photocatalyst particles. Phenol concentration was measured chromatographically. HPLC system included chromatograph Shimadzu LC-6A, WAKOSIL-II 5C18 AR column (dimensions 4.6 mm × 250 mm) and detector UV-vis Shimadzu SPD-6A with detection wavelength at 254 nm. Mobile phase for analysis contained water, acetonitrile and phosphoric acid in volume ratio of 70:29.5:0.5. In order to evaluate photocatalytic mechanism, action spectrum measurements were performed. Suspension of photocatalyst and phenol solution was irradiated by monochromatic light emitted by diffraction grating type illuminator with a 300-W xenon lamp. Apparent quantum efficiency was calculated in order to 1,4-benzoquinone (BQ) generation. Concentration of BQ was evaluated using the HPLC system.

5. Conclusions

On the basis of these results it could be stated that the photocatalytic activity of Pt-TiO_2 composites under UV and visible light was strongly affected by the morphology of platinum nanoparticles deposited on the surface of TiO_2. The enhanced photoactivity lied crucially on the contribution role of platinum particles acting as electron reservoir in prolonging the lifetime of photogenerated charge carriers'. Firstly, the interaction between metal-TiO_2 formed at the interface before reduction of platinum ions was crucial for preparation of Pt particles with defined morphology by the simple wet-impregnation method without using any stabilizer or surfactant. Moreover, the photoactivity of Pt-modified TiO_2 samples could be related to (i) the different content of Pt(0)/Pt(σ+), (ii) the amount of surface defects such as oxygen vacancies, (iii) the type of facets {101} or {001} for efficient electron transfer and charge carriers' separation. Furthermore, the microemulsion method enabled us to control the Pt particle properties such as geometry, morphology and homogeneity by varying the value water to surfactant molar ratio. For the obtained samples with the same Pt size (5–6 nm) defined as mean particle diameter in TEM images and crystallite size of Pt (111) calculated based on Scherrer formula, which were deposited on different TiO_2 supports the photoactivity was almost the same. Therefore, it was confirmed that the photoactivity mainly depended on platinum size deposited on different TiO_2 templates almost regardless of the TiO_2 properties. In view of this, it can be assumed that the tight control of Pt morphology allows us to design highly active materials with enhanced photocatalytic performance.

Author Contributions: Conceptualization, A.Z.-J.; Formal analysis, A.Z.-J., Z.W. and M.J.; Funding acquisition, A.Z.-J.; Investigation, A.Z.-J. and I.W.; Methodology, A.Z.-J. and E.K.; Project administration, A.Z.-J.; Writing—original draft, A.Z.-J.; Writing—review and editing, A.Z.-J. and E.K.

Funding: This research was funded by Polish National Science Center grant number NCN 2016/23/D/ST5/01021) and Polish Ministry of Science and Higher Education grant no. 0525/E-359/STYP/13/2018.

Acknowledgments: This research was supported by Polish National Science Centre, grant no. NCN 2016/23/D/ST5/01021) and Polish Ministry of Science and Higher Education grant no. 0525/E-359/STYP/13/2018—Scholarships for outstanding young scientists.

Conflicts of Interest: The authors declare no conflict of interest.

References:

1. Tryba, B. Immobilization of TiO_2 and Fe-C-TiO_2 photocatalysts on the cotton material for application in a flow photocatalytic reactor for decomposition of phenol in water. *J. Hazard. Mater.* **2008**, *151*, 623–627.
2. Zhang, G.; Choi, W.; Kim, S.H.; Hong, S.B. Selective photocatalytic degradation of aquatic pollutants by titania encapsulated into FAU-type zeolites. *J. Hazard. Mater.* **2011**, *188*, 198–205.
3. Benoit-Marquié, F.; Wilkenhöner, U.; Simon, V.; Braun, A.M.; Oliveros, E.; Maurette, M.T. VOC photodegradation at the gas–solid interface of a TiO2 photocatalyst Part I: 1-butanol and 1-butylamine. *J. Photochem. Photobiol. A Chem.* **2000**, *132*, 225–232.
4. Lu, N.; Yu, H.T.; Su, Y.; Wu, Y. Water absorption and photocatalytic activity of TiO2 in a scrubber system for odor control at varying pH. *Sep. Purif. Technol.* **2012**, *90*, 196–203.
5. Zielińska-Jurek, A.; Wei, Z.; Wysocka, I.; Szweda, P.; Kowalska, E. The effect of nanoparticles size on photocatalytic and antimicrobial properties of Ag-Pt/TiO_2 photocatalysts. *Appl. Surf. Sci.* **2015**, *353*, 317–325.
6. Folli, A.; Pade, C.; Hansen, T.B.; de Marco, T.; Macphee, D.E. TiO2 photocatalysis in cementitious systems: Insights into self-cleaning and depollution chemistry. *Cem. Concr. Res.* **2012**, *42*, 539–548.
7. Zhu, M.; Han, M.; Zhu, C.; Hu, L.; Huang, H.; Liu, Y.; Kang, Z. Strong coupling effect at the interface of cobalt phosphate-carbon dots boost photocatalytic water splitting. *J. Colloid Interface Sci.* **2018**, *530*, 256–263.
8. Razalia, M.H.; Yusoff, M. Highly efficient CuO loaded TiO_2 nanotube photocatalyst for CO_2 photoconversion. *Mater. Lett.* **2018**, *221*, 168–171.
9. Sugishita, N.; Kuroda, Y.; Ohtani, B. Preparation of decahedral anatase titania particles with high-level photocatalytic activity. *Catal. Today* **2011**, *164*, 391–394.
10. Janczarek, M.; Kowalska, E.; Ohtani, B. Decahedral-shaped anatase titania photocatalyst particles: Synthesis in a newly developed coaxial-flow gas-phase reactor. *Chem. Eng. J.* **2016**, *289*, 502–512.
11. Asahi, R.; Morikawa, T.; Ohwaki, T.; Aoki, K.; Taga, Y. Visible-light photocatalysis in nitrogen-doped titanium oxides. *Science* **2001**, *293*, 269–271.
12. Zielińska-Jurek, A.; Klein, M.; Hupka, J. Enhanced visible light photocatalytic activity of Pt/I-TiO_2 in a slurry system and supported on glass packing. *Sep. Purif. Technol.* **2017**, *189*, 246–252.
13. Roberts, P.H.; Thomas, K.V. The occurrence of selected pharmaceuticals in wastewater effluent and surface waters of the lower Tyne catchment. *Sci. Total Environ.* **2006**, *356*, 143–153.
14. Verbruggen, S.W.; Keulemans, M.; Goris, B.; Blommaerts, N.; Bals, S.; Martens, J.A.; Lenaerts, S. Plasmonic 'rainbow' photocatalyst with broadband solar light response for environmental applications. *Appl. Catal. B Environ.* **2016**, *188*, 147–153.
15. Wei, Z.; Janczarek, M.; Endo, M.; Colbeau-Justin, C.; Ohtani, B.; Kowalska, E. Silver-modified octahedral anatase particles as plasmonic photocatalyst. *Catal. Today* **2018**, *310*, 19–25.
16. Nahar, S.; Hasan, M.R.; Kadhum, A.A.H.; Hasan, H.A.; Zain, M.F.M. Photocatalytic degradation of organic pollutants over visible light active plasmonic Ag nanoparticle loaded Ag2SO3 photocatalysts. *J. Photochem. Photobiol. A Chem.* **2019**, doi:10.1016/j.jphotochem.2019.02.025.
17. Zielińska-Jurek, A. Progress, challenge and perspective of bimetallic TiO2-based photocatalysts. *J. Nanomater.* **2014**, doi:10.1155/2014/208920.
18. Chen, H.W.; Ku, Y.; Kuo, Y.L. Effect of Pt/TiO2 characteristics on temporal behavior of o-cresol decomposition by visible light-induced photocatalysis. *Water Res.* **2007**, *41*, 2069–2078.
19. Zielińska-Jurek, A.; Hupka, J. Preparation and characterization of Pt/Pd-modified titanium dioxide nanoparticles for visible light irradiation. *Catal. Today* **2013**, *230*, 181–187.
20. Litke, A.; Frei, H.; Hensen, E.J.M.; Hofmann, J.P. Interfacial charge transfer in Pt-loaded TiO_2 P25 photocatalysts studied by in-situ diffuse reflectance FTIR spectroscopy of adsorbed CO. *J. Photochem. Photobiol. A Chem.* **2019**, *370*, 84–88.
21. Xiong, Z.; Lei, Z.; Chen, X.; Gong, B.; Zhao, Y.; Zhang, J.; Zheng, C.; Wu, J.C.S. CO_2 photocatalytic reduction over Pt deposited TiO2 nanocrystals with coexposed {101} and {001} facets: Effect of deposition method and Pt precursors. *Catal. Commun.* **2017**, *96*, 1–5.
22. Sun, B.; Vorontsov, A.V.; Smirniotis, P.G. Role of platinum deposited on TiO2 in phenol photocatalytic oxidation. *Langmuir* **2003**, *19*, 3151–3156.
23. Wu, S.; Tan, X.; Liu, K.; Lei, J.; Wang, L.; Zhang, J. TiO2 (B) nanotubes with ultrathin shell for highly efficient photocatalytic fixation of nitrogeni. *Catal. Today* **2018**, doi:10.1016/j.cattod.2018.11.043.
24. Kowalska, E.; Wei, Z.; Karabiyik, B.; Herissan, A.; Janczarek, M.; Endo, M.; Markowska-Szczupak, A.; Remita, H.; Ohtani, B. Silver-modified titania with enhanced photocatalytic and antimicrobial properties under UV and visible light irradiation. *Catal. Today* **2015**, *252*, 136–142.

25. Ohtani, B.; Prieto-Mahaney, O.O.; Li, D.; Abe, R. What is Degussa (Evonik) P25? Crystalline composition analysis, reconstruction from isolated pure particles and photocatalytic activity test. *J. Photochem. Photobiol. A Chem.* **2010**, *216*, 179–182.
26. Luo, Z.; Poyraz, A.S.; Kuo, C.H.; Miao, R.; Meng, Y.; Chen, S.Y.; Jiang, T.; Wenos, C.; Suib, S.L. Crystalline mixed phase (anatase/rutile) mesoporous titanium dioxides for visible light photocatalytic activity. *Chem. Mater.* **2015**, *27*, 6–17.
27. Zhao, H.; Liu, L.; Andino, J.M.; Li, Y. Bicrystalline TiO2 with controllable anatase-brookite phase content for enhanced CO2 photoreduction to fuels. *J. Mater. Chem. A* **2013**, *1*, 8209–8216.
28. Kitchens, C.L.; McLeod, M.C.; Roberts, C.B. Chloride ion effects on synthesis and directed assembly of copper nanoparticles in liquid and compressed alkane microemulsions. *Langmuir* **2005**, *21*, 5166–5173.
29. Han, Y.; Liu, C.J.; Ge, Q.; Effect of surface oxygen vacancy on Pt cluster adsorption and growth on the defective anatase TiO2 (101) surface. *J. Phys. Chem. C* **2007**, *111*, 16397–16404.
30. Cueto, M.; Piedrahita, M.; Caro, C.; Martínez-Haya, B.; Sanz, M.; Oujja, M.; Castillejo, M. Platinum nanoparticles as photoactive substrates for mass spectrometry and spectroscopy sensors. *J. Phys. Chem. C* 2014, 118, 11432–11439.
31. Jung, S.; Shuford, K.L.; Park, S. Optical property of a colloidal solution of platinum and palladium nanorods: Localized surface plasmon resonance. *J. Phys. Chem. C* **2011**, *115*, 19049–19053.
32. Kowalska, E.; Abea, R.; Ohtani, B. Visible light-induced photocatalytic reaction of gold-modified titanium(IV) oxide particles: Action spectrum analysis. *Chem. Commun.* **2009**, *2*, 241–243.
33. Galhenage, R.P.; Yan, H.; Tenney, S.A.; Park, N.; Henkelman, G.; Albrecht, P.; Mullins, D.R.; Chen, D.A. Understanding the nucleation and growth of metals on TiO2: Co compared to Au, Ni, and Pt. *J. Phys. Chem. C* **2013**, *117*, 7191–7201.
34. Campbell, C.T. Ultrathin metal films and particles on oxide surfaces: Structural, electronic and chemisorptive properties. *Surf. Sci. Rep.* **1997**, *27*, 1–111.